Anisotropically splayed and columnar defects in untwinned $YBa_2Cu_3O_{7-\delta}$

W. K. Kwok
Materials Science and Science and Technology Center for Superconductivity, Argonne National Laboratory, Argonne, Illinois 60435

L. M. Paulius
Department of Physics, Western Michigan University, Kalamazoo, Michigan 49008

V. M. Vinokur
Materials Science and Science and Technology Center for Superconductivity, Argonne National Laboratory, Argonne, Illinois 60435

A. M. Petrean
Department of Physics, Western Michigan University, Kalamazoo, Michigan 49008

R. M. Ronningen
National Superconducting Cyclotron Laboratory, Michigan State University, East Lansing, Michigan 48824

G. W. Crabtree
Materials Science and Science and Technology Center for Superconductivity, Argonne National Laboratory, Argonne, Illinois 60435
(Received 26 March 1998)

Pinning by splayed and columnar defects created by 3.9 GeV $^{197}Au^{29+}$ ions is investigated using transport measurements of vortex motion perpendicular and parallel to the splay plane in untwinned crystals of $YBa_2Cu_3O_{7-\delta}$. These results are compared with a sample with parallel columnar defects parallel to the *c* axis. We report on the temperature, field, and angular dependence of the vortex liquid and solid state. We find that, at twice the matching field, the irreversibility lines for pre- and post-irradiated splayed-defect samples cross. We determine the vortex liquid pinning energy for splayed and columnar defects and show that the barrier to vortex motion perpendicular to the splay plane is greater than that to motion parallel to the splay plane. [S0163-1829(98)01646-4]

INTRODUCTION

The search for the optimum vortex pinning configuration in high temperature superconductors continues to be of great interest due to its technological importance. In this work we report studies of the pinning effects of splayed columnar defects introduced into untwinned single crystals of $YBa_2Cu_3O_{7-\delta}$. Correlated defects in the form of columnar tracks induced by heavy ion irradiation have so far yielded the most noteworthy pinning enhancement by shifting the irreversibility line to higher temperatures and increasing the critical current at both high temperatures and high fields.[1,2] Pinning can be controlled by the irradiation fluence (which can be related to a dose equivalent ''matching field'' B_Φ where the number of columnar defects equals the number of vortices), thereby optimizing the magnetic field range over which pinning is enhanced. Other previous experimental approaches have included: inclusion of secondary phase material into the parent compound,[3] controlled introduction of point defects via electron[4–6] and proton irradiation;[7,8] cascade defect pinning induced by neutron irradiation.[9] In many cases, an enhancement of the critical current has been observed. A vortex glass state,[10,11] for randomly distributed weak point defects, and a Bose glass state,[12,13] for correlated defects, have been proposed to explain the vortex-pin site interactions in the vortex solid state.

More recently, it has been predicted that a splayed geometry created by heavy ion irradiation at different angles[14] would further enhance the pinning capabilities of correlated columnar defects. The splay geometry induces orientational confusion in the vortex array, promoting topological entanglement of the vortices as they bend to follow the different pinning directions. This topologically *entangled* splay glass ground state could have stronger pinning than the *unentangled* Bose glass state. Experiments on the natural splay created by heavy ions traveling through thick samples[15] and random splay created by fissioning the Bi atoms in $Bi_2Sr_2CaCu_2O_{8+\delta}$ via high energy protons[16–18] have verified some of these predictions. Further experiments comparing fixed angle splay to Gaussian splay[19,20] suggest that the former enhances the critical current while the latter promotes flux creep.

Here, we irradiated untwinned single crystals of $YBa_2Cu_3O_{7-\delta}$ with heavy ions at two fixed angles defining a plane containing the crystallographic *c* axis (see inset to Fig. 1). The splayed columnar defects created by this procedure form a two dimensional barrier which, like a twin boundary, would appear very different to vortices moving parallel or perpendicular to the barrier.[21] However, previous experiments, which were performed on twinned samples, were unable to separate the effects of linear or splayed columnar defects from the effects of the twin planes. We used well characterized untwinned single crystals of $YBa_2Cu_3O_{7-\delta}$ which showed clear first order vortex solid to liquid transi-

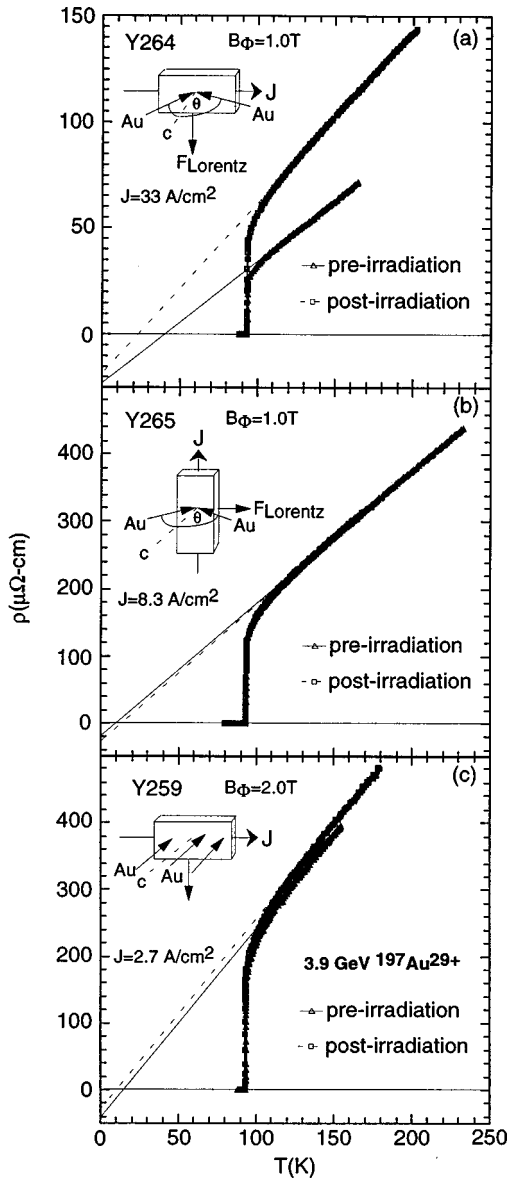

FIG. 1. Zero field superconducting resistive transitions before and after irradiation for two splayed defect crystals, (a) Y264 and (b) Y265, and one columnar defect crystal (c) Y259. Inset shows the irradiation geometry and the relative direction of the induced Lorentz force. The lines are extrapolations of the normal state resistivity above 120 K to zero temperature, depicting the negative intercept before irradiation (lines) and after irradiation (dashed line).

tions. We performed extensive transport measurements of the effect of the Lorentz force on the vortex pinning behavior for motion parallel and perpendicular to the splay plane in the presence of an applied magnetic field along the crystallographic *c* axis. A brief account of our results was presented in an earlier publication.[22]

Remarkably, the irreversibility lines of the pre-irradiated and post-irradiated splayed samples cross at nearly twice the matching field. In contrast, the irreversibility lines in a sample irradiated with parallel columnar defects along the *c* axis do not cross. A close investigation of the vortex liquid state in both splayed and parallel columnar defect samples shows several characteristic features related to the dose matching field. They include a maximum shift of the irreversibility line after irradiation occurring at the matching field, a sharp increase in the onset of vortex liquid pinning and an increase in the pinning accommodation angle just below the matching field. In addition, the measured pinning energy in the vortex liquid state exceeds the theoretical vortex cutting energy[23] in these samples, indicating that the splayed columnar defects effectively pin the vortex liquid because it is topologically entangled. We determined the vortex liquid pinning energy using an interpolation formula and find that it follows an inverse field dependence which can be explained by a *vortex lace* model which is based on the premise that a highly entangled vortex system can be held together by a few strong pinning centers. Furthermore, we show that in the vortex liquid state, for magnetic fields below the matching field, pinning is anisotropic, depending upon whether the vortex motion is parallel or perpendicular to the splay planes. We determine the onset temperature of splayed columnar defect pinning in the liquid state using angular dependent magnetoresistance and a comparison of the resistive state before and after irradiation. We find that, in the vortex liquid state, *isotropic* pinning precedes the onset of *anisotropic* pinning for magnetic fields below the matching field. In the vortex solid state, we demonstrate that the critical current for vortex motion perpendicular to the splay plane increases with decreasing temperature at three times the rate at which motion parallel to the splay plane increases. Our studies also yielded information concerning pinning in the unirradiated state. For example, we observed a precursor peak effect just below the melting temperature in the unirradiated untwinned crystal. The peak effect results from vortex shear modulus softening prior to melting which gives rise to enhanced pinning, which in this case originates from very weak remnant strain fields resulting from the detwinning process of the crystal. For off axis magnetic field pinning, the peak effect is related to enhanced pinning from isotropic point defects.

SAMPLE PREPARATION AND EXPERIMENTAL SETUP

The samples were grown by a self flux method described elsewhere[24] which yielded small platelet single crystals with twin boundaries of various densities along the $\langle 110 \rangle$ and $\langle 1\bar{1}0 \rangle$ directions. Two crystals were prepared for irradiation with splayed columnar defects. The crystals were detwinned[25] by annealing at ~450 °C under uniaxial pressure along one of the **a/b** crystallographic axes. Polarized light microscopy showed no evidence of twins after the detwinning process. Based on TRIM analysis,[26] the crystals were subsequently polished down to a thickness of 20 μm to ensure that the heavy ions would traverse linearly through the entire thickness of the sample. The final dimensions of the two crystals were: $0.15(w)\times 0.9(l)\times 0.02(t)$ mm^3 (crystal Y264) and $0.6(w)\times 0.8(l)\times 0.02(t)$ mm^3 (crystal Y265) with length l parallel to the crystallographic *b* axis. These crystals are compared to a third untwinned crystal (Y259), with dimensions $0.18(w)\times 0.98(l)\times 0.02(t)$ mm^3, irradiated with heavy ions to form columnar defects parallel to the crystallographic *c* axis. Gold wires were attached to the samples with silver epoxy, resulting in contact resistance of less than 1Ω. The resistivity was measured by the standard

TABLE I. Pre- and post-irradiation characteristics in zero field.

	T_{c0}		ΔT_{c0} (10–90 %)		$d\rho/dT$ ($\mu\Omega$ cm/K)		ρ_0 ($\mu\Omega$ cm)		ρ_n (95 K) ($\mu\Omega$ cm)	
Crystals	pre-	post-	pre-	post-	pre-	post-	pre-	post-	pre-	post-
Y264	93.46 K	93.46 K	230 mK	310 mK	0.583	0.80	−24.4	−17.91	27.0	47.68
Y265	93.55 K	93.44 K	260 mK	260 mK	1.99	2.06	−21.1	−32.0	131.5	133.9
Y259	93.47 K	93.17 K	300 mK	320 mK	2.82	2.85	−40.39	−29.49	180.2	197.2

four probe technique using either a dc current or an ac current at 23 Hz applied in the Cu-O plane of the crystal. Typical measuring current densities ranged from 0.08 A/cm^2 to 60 A/cm^2. The samples were placed in the bore of a 1.5 T superconducting split coil magnet which resides in the center of an 8 T superconducting solenoid. The resultant field was determined by the fields of the two orthogonal magnets and enabled the magnetic field to be rotated with very high precision $\Delta\theta < 0.001°$ with virtually no hysteresis.

Crystals Y264 and Y265 were irradiated with 3.9 GeV $^{197}Au^{29+}$ ions at the National Superconducting Cyclotron Laboratory (NSCL) with a splay angle of $\pm 10°$ from the crystallographic c axis to a matching field of $B_\Phi = 0.5$ T along each direction. (See inset diagrams in Fig. 1.) The irradiation geometry of Y264 produced a splay plane parallel to the current direction, inducing a Lorentz force $F_L = (1/c)J \times \Phi$ perpendicular to the splay plane for an applied magnetic field along the crystallographic c axis. In Y265, the induced Lorentz force was parallel to the splay plane. Crystal Y259 was irradiated earlier to a matching field of $B_\Phi = 2.0$ T with the same ions along the crystallographic c axis to create parallel columnar defects.

A. Effects of irradiation in zero magnetic field

The values of the zero field transition temperature, T_{c0}, the width of the transition, ΔT_{c0}, the slope of the normal state resistivity ($d\rho/dT$), the linearly extrapolated normal state resistivity intercept at T_{c0}, (ρ_0), and the normal state resistivity $\rho_n(T = 95\ \mathrm{K})$ before and after irradiation are summarized in Table I. In general, irradiation damage in these crystals is marked by a slight decrease in T_{c0} and an increase in ΔT_{c0} and the normal state resistivity. The decrease in T_{c0} and the increase in ρ_n are not as dramatic as those observed in untwinned crystals irradiated with uranium ions,[27] suggesting that ion size may play a role in the severity of damage inflicted by irradiation.

Figure 1 shows the resistive transitions for crystals Y264, Y265, and Y259 before and after irradiation measured with a current density ranging from 0.83 A/cm^2 to 33 A/cm^2. The high quality of the crystals is evidenced by their high ($T_{c0} > 93.0$ K) and sharp ($\Delta T_{c0} \leqslant 300$ mK) preirradiation zero-field transition temperatures. The transition temperatures of the crystals were determined from the peak in the derivative of the zero field temperature dependence of the resistivity. All the crystals displayed a linear normal state temperature dependent resistivity which extrapolated to negative values, a feature usually indicative of high quality crystals. The postirradiation curves also show similar characteristics. Furthermore, the zero field resistive transitions after irradiation decreased by less than 300 mK in all cases. For two of the crystals, Y265 and Y259, the normal state resistivity increased by only a few percent, while for Y264 it increased by ~40%. This crystal also displayed the lowest normal state resistivity, suggesting that the cleanest crystals are most susceptible to damage by irradiation.

B. Vortex liquid pinning and the irreversibility line

We investigate below, the behavior of the vortex liquid state before and after irradiation in the presence of a magnetic field along the crystallographic c axis ($H \| c$). From the temperature dependence of the resistivities we obtain the vortex lattice melting line before irradiation, the pre- and postirradiation irreversibility lines and the vortex liquid state pinning energy for vortex motion perpendicular and parallel to the splay plane. Furthermore, we find a peak effect in one of the unirradiated samples related to pinning by anisotropic defects near $H \| c$ and by isotropic defects away from $H \| c$, which shows evidence against geometrical barrier pinning in $YBa_2Cu_3O_{7-\delta}$ crystals, at least at high magnetic fields.

Figure 2 shows the resistive transition as a function of temperature for Y264 before irradiation in magnetic fields up to 8 T applied parallel to the crystallographic c axis. We find a sharp ''kink'' at the tail of the resistive transition for all fields up to $H = 8$ T. This ''kink'' is associated with a first order vortex solid to liquid melting transition usually observed in clean untwinned crystals.[28–30] The inset to Fig. 2

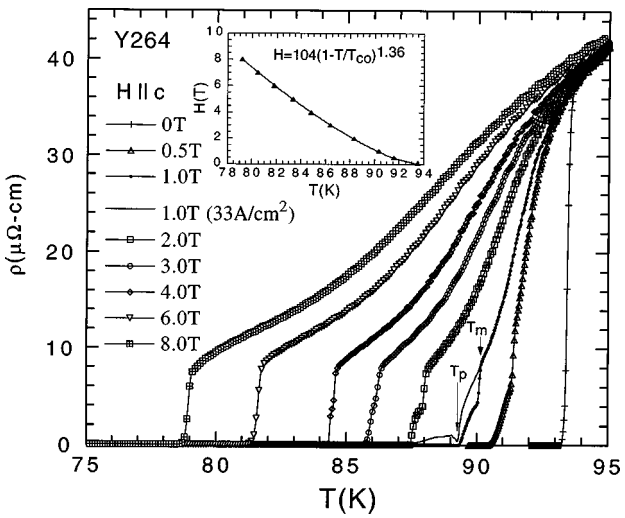

FIG. 2. Temperature dependence of the resistivity in finite fields for Y264. T_m and T_p indicate the vortex lattice melting temperature and the peak effect temperature respectively. Note the two measuring currents $J = 3.3$ A/cm^2 and 33 A/cm^2 for $H = 1$ T. Inset: Magnetic phase diagram showing the vortex lattice melting line for this crystal.

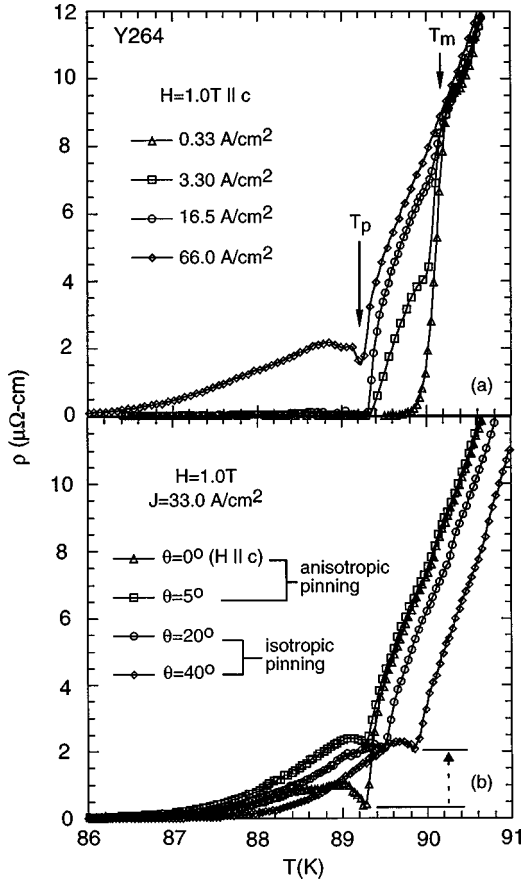

FIG. 3. Tail of the resistive transition of Y264 for $H=1\ \mathrm{T}\|c$ for (a) different measuring currents, and (b) tilt angles of the magnetic field with respect to the c axis.

shows the magnetic phase diagram depicting the vortex lattice melting line for Y264. The melting temperature was determined from the onset of the ''kink'' in the resistivity. The data can be fitted with $H=H_0(1-T/T_{c0})^{\alpha}$, where $H_0=105$ T and $\alpha=1.37\pm0.01$, consistent with values obtained in other high quality untwinned crystals.[29,31]

At high measuring current densities we observed a peak effect in the critical current. The data in Fig. 2 were obtained with a measuring current density of 3.3 A/cm^2. At this measuring current, we observed a second ''step'' just below the ''kink'' for $H\leqslant 2$ T. At higher fields, only one sharp transition is observed at T_m. The non-Ohmic region begins just below the ''kink'' as shown by the deviation at $T_m=90.0$ K between the two resistive curves for $H=1.0$ T, obtained with a measuring current density of $J=3.3$ A/cm^2 and 33 A/cm^2 respectively. For the latter curve, we observe a resistive minimum at $T_p=89.25$ K. This minimum occurs in the non-Ohmic regime and implies a ''peak effect'' [32–35] in the critical current.

In order to further investigate the peak effect, we plot the tail end of the resistive transition as a function of temperature for $H=1\ \mathrm{T}\|c$ for various measuring current densities in Fig. 3(a). For low excitation currents, $J=0.33$ A/cm^2, we observe only a single ''kink'' at the vortex lattice melting transition. Increasing the measuring current by an order of magnitude to 3.3 A/cm^2 yields another ''step'' just below T_m. With further increase in the current, the height of the ''step'' increases and merges into a single broad ''kink'' at T_m. This is clearly shown for $J=66$ A/cm^2, where the height of the ''step'' approaches the ''kink'' at T_m and a pronounced ''peak effect'' or dip in the resistivity becomes evident about 0.5 K below the melting temperature at $T_p=89.20$ K. In previous reports comparing transport measurements with magnetization measurements, the ''kink'' in the resistive transition has been associated with a thermodynamic vortex melting transition which occurs at the onset of the ''kink'' at T_m, where a corresponding jump in the magnetization is also observed.[36] There, it was shown that the width of the jump in the magnetization is independent of the broadening of the resistive transition below the kink with increasing measuring current. These results suggest that the broadening is due to vortex flow in the solid state when the measuring current exceeds the depinning current. The ''step'' and the minimum in the resistivity just below the melting transition is indicative of enhanced pinning arising from the elastic distortion of the ''soft'' vortex lattice to accommodate favorable pinning sites.[34] We can gain some insight to the nature of the pinning site by tilting the magnetic field with respect to the c axis.

Figure 3(b) shows the same $H=1.0$ T resistive transition for Y264 for several different magnetic field orientations (θ) with respect to the c axis. A tilt of only 5° off the c axis decreases the depth of the dip at T_p, thus reducing the resistive ''peak effect.'' This suggests that the pinning site is highly anisotropic. However, a small remnant resistive dip with constant depth is still visible up to $\theta=40°$, which indicates that at tilt angles greater than 5°, the pinning becomes isotropic. The peak effect at $\theta=0°$ is probably due to residual strain fields in the detwinned crystal. Although no twin boundaries were observed by polarized light microscopy, a small strain field may remain at the sites of the former twin boundaries. The weakness of the strain field is underlined by its small pinning accommodation angle θ_{acc} of less than 5° (in densely twinned samples, $\theta_{\mathrm{acc}}>25°$) and its occurrence only in the vortex solid phase where a finite shear modulus enhances the pinning. The isotropic pinning at $\theta>5°$ probably comes from point defects such as oxygen disorder. We can rule out surface barriers,[37] since rotating the magnetic field with respect to the crystal does not seem to change the depth of the dip. If surface barriers were important, we would expect to see a change in this height since the geometry of the magnetic field with respect to the crystal surface for a platelet sample changes considerably with rotation, and would thus affect the pinning.

Y264 was irradiated with 3.9 GeV $^{197}Au^{29+}$ ions in a splay geometry with incident angles of $\theta=\pm10°$ from the c axis. The fluence was equivalent to a matching field of $B_\Phi=0.5$ T in each direction, resulting in a total matching field of $B_\Phi=1$ T. With $J\|b$ and $H\|c$, a Lorentz force is induced on the vortices in a direction perpendicular to the splay defect plane. The normalized resistivity $\rho/\rho(T_{c0})$ for Y264 as a function of reduced temperature $t=T/T_{c0}$ for several magnetic fields after irradiation (thick lines) is shown in Fig. 4(a). For comparison we include the preirradiation data (thin lines) from Fig. 2. The measuring current is 3.3 A/cm^2 for both sets of resistivity curves. In contrast to the preirradiation temperature dependence, the sharp ''kink'' associated with the vortex melting transition is absent. Furthermore,

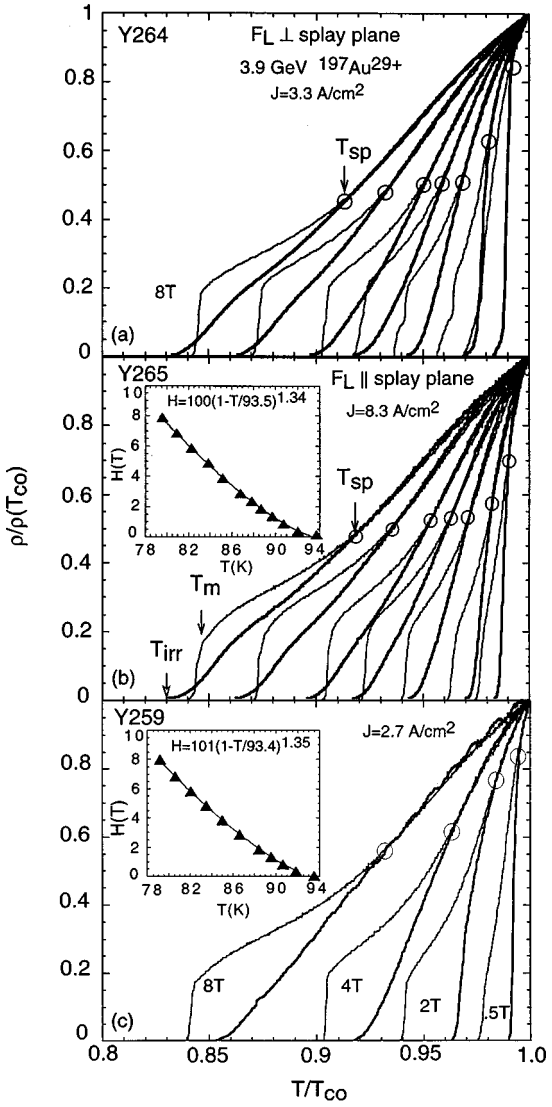

FIG. 4. Comparison of the temperature dependence of the resistivity in finite magnetic fields before (thin lines) and after (thick lines) irradiation for (a) Y264 and (b) Y265 at $H=0.5$, 1, 2, 3, 4, 6, and 8 T$\|c$ and for (c) Y259 at $H=0.5$, 2, 4, and 8 T$\|c$. The circles at T_{sp} depict the onset of pinning, resulting from heavy ion irradiation. Inset: Magnetic phase diagram for Y265 and Y259 showing the vortex lattice melting line.

unlike the behavior observed in the preirradiation crystal, the curves display Ohmic behavior throughout the entire transition. At fields greater than $H=4$ T, a bump in the tail of the resistive transition begins to develop, becoming a more obvious ''shoulder'' at $H=8$ T. This ''shoulder'' is similar to those observed in electron irradiated untwinned crystals of $YBa_2Cu_3O_{7-\delta}$[6] and suggests that point defects may become important at $H>B_\Phi$ and at lower temperatures.

Another salient difference is the zero resistance temperature. For $H<3$ T, the resistivity for the irradiated sample goes to zero at a higher temperature than that for the unirradiated sample, indicating that pinning is enhanced after irradiation. However, for $H>3$ T, the zero resistivity point for the unirradiated case lies above that of the irradiated case, indicating a reversal in the pinning behavior. The normalized resistivity plot allows us to identify the onset of pinning in the vortex liquid state as the separation point between the unirradiated and irradiated resistivity curves, designated by T_{sp}, and indicated by a circle in Fig. 4. For $H>B_\Phi$, the resistive onset of pinning occurs near $\rho/\rho_n\sim0.5$, much higher than the values obtained for twin boundary pinning in $YBa_2Cu_3O_{7-\delta}$ where $\rho/\rho_n\sim0.25$.[21] Furthermore, for $H\leqslant B_\Phi=1$ T, the resistive onset of pinning due to splayed defect increases sharply and reaches a value of $\rho/\rho_n\sim0.85$ at $H=0.5$ T.

Figure 4(b) shows similar results for crystal Y265 before (thin lines) and after (thick lines) irradiation. Here, the crystal was irradiated to produce splay in the *ac* plane, giving a Lorentz force parallel to the splay defect plane for a measuring current along the *b* axis and an applied field along the *c* axis. A sharp kink in the tail of the superconducting transition related to the vortex lattice melting transition is also found in this crystal. However, we observed no ''peak effect'' or minimum in the resistivity tail at large driving currents as was shown in Fig. 3 for Y264. The inset to Fig. 4(b) shows the vortex lattice melting line for this crystal before irradiation, determined from the onset of the ''kink'' in the resistivity. The data can be fit with $H=H_0(1-T/T_{c0})^\alpha$, where $H_0=100$ T and $\alpha=1.34\pm0.01$, very similar to the values obtained for Y264. After irradiation, the first order melting transition is completely suppressed and replaced by a smooth ''Ohmic'' transition similar to that shown in Fig. 4(a) for Y264. The onset of pinning at T_{sp} also follows the same behavior observed in Y264. Here, the onset rises to about $\rho/\rho_n\sim0.7$ for $H=0.5$ T. Moreover, the reversal of the zero resistance point defined here as T_{im}, at nearly twice the matching field is also similar to that observed in Y264.

Finally, Fig. 4(c) shows the comparison of the resistivity before and after irradiation for Y259 which was irradiated along the crystallographic *c* axis with a fluence of $B_\Phi=2.0$ T, creating *parallel* columnar defects. Here, the zero resistance temperature for the irradiated case is always higher than the unirradiated case. Thus no reversal of the pinning behavior is observed in this crystal. On the other hand, the resistive onset of pinning in the vortex liquid state, $\rho/\rho(T_{c0})(T_{sp})$, determined from the deviation of the normalized resistivity curves before and after irradiation, also increases to a higher value for magnetic fields $H\leqslant B_\Phi$, similar to Y264 and Y265. The inset shows the vortex lattice melting curve for Y259. The data is fitted to $H_m=101(1-T/T_{c0})^{1.35}$, consistent with the values obtained for both Y264 and Y265 before irradiation.

We determined the irreversibility lines before and after irradiation for the three crystals from the zero resistivity temperature, using a resistive criterion of $\rho=0.01$ $\mu\Omega$ cm, the resolution of our instrumentation. The irreversibility lines shown in Figs. 5(a) and 5(b) for Y264 and Y265 respectively, clearly depict the pinning reversal behavior mentioned above as a crossing of the irreversibility lines at nearly twice the matching field. This suggests that splayed defects increase pinning in the vortex liquid state only for fields less than about $2B_\Phi$. In contrast, no crossing of the irreversibility lines is observed for Y259, irradiated with parallel columnar defects. The maximum shift in the irreversibility lines after irradiation occurs near the matching field, $B_\Phi=1$ T, for Y264 and Y265, and near $B_\Phi=2$ T for Y259.

The depression of the post-irradiation irreversibility line with respect to the first order vortex melting line above H

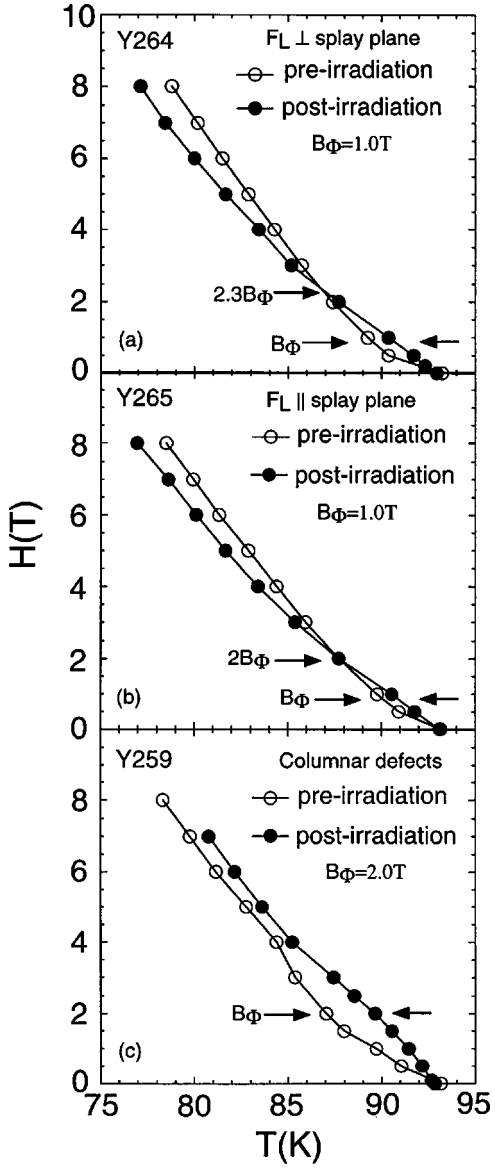

FIG. 5. The irreversibility lines before and after irradiation for the splayed defect crystals, (a) Y264 and (b) Y265 and for the columnar defect crystal (c) Y259 for magnetic fields parallel to the c axis.

$=2B_\Phi$ in the splayed defect crystals (Y264 and Y265), is similar to the behavior of the irreversibility line observed in electron irradiated untwinned single crystals.[6] There, it was speculated that the depression is caused by an entangled vortex liquid state induced by driving vortex lines through a random point pinning environment which may give rise to formation of a polymerlike glass state at temperatures below the first order vortex melting transition. The ''plastic energy,'' $U_{\rm pl}$, associated with vortex cutting and recombination in an entangled liquid was measured in that study to be of the order of $U_{\rm pl}/k_B \sim 800$ K at $T=83$ K and $H=5$ T.

Using a similar analysis, we can extract the temperature dependent dissipation in the vortex liquid state due to splayed columnar defects using the interpolation formula $\rho = (1/\rho_f + 1/\rho_{\rm sp})^{-1}$ where ρ is the post-irradiation resistivity value, $\rho_{\rm sp}$ is the resistivity due to splayed defects, ρ_f is the preirradiation flux flow resistivity. This interpolation formula is based on the assumption that the vortex system is a viscous liquid above T_m and thus its resistivity can be expressed as $\rho=\rho_f/(1+\delta v/v)$ where $\delta v/v$ is the relative velocity change related to the viscosity of the vortex liquid.[38] For Y265, at $H=1$ T, we fit the temperature range between $0.974<t<0.983$ in the vortex liquid regime between the onset of the splayed defect pinning $T_{\rm sp}$ and the preirradiation melting temperature T_m [see Fig. 4(b)]. The linear behavior of the curve shown in Fig. 6 for both Y264 and Y265 indicates that $\rho_{\rm sp}$ follows an exponential behavior described by $\rho_{\rm sp}=\rho_0 \exp[-U(1-t)/t]$. A linear fit to the data of Y265 for $H=1$ T yields $U_{\rm po}/k_B=49821$ K. At $T=91$ K, near the irreversibility line for $B_\Phi=1$ T, $U_p(91\ {\rm K})=U_{\rm po}(1-t)=1280$ K. Two distinct regimes of exponential behavior are observed for magnetic fields above $2B_\Phi$. We determined the field dependence of the vortex liquid pinning potential by fitting only the high temperature behavior, since the low temperature region may be influenced by the appearance of the ''shoulder'' mentioned earlier in the postirradiation resistivity curves. Figure 7 shows the field dependence of $U_p(T=91\ {\rm K})$ for Y264, Y265, and Y259. The curves follow a $1/H$ dependence, unlike the $Up \sim \varepsilon\varepsilon_0 a_0 \sim 1/H^{1/2}$ behavior predicted for vortex liquid flow[38,39] nor the $H^{-0.7}$ dependence observed in electron irradiated samples.[6] The curve for Y264 lies above the curve for Y265, indicating that the vortex liquid pinning energy for vortex motion perpendicular to the splay plane is greater than the pinning energy for vortex motion parallel to the splay plane. The curve for Y259 also follows a $1/H$ behavior. Although this crystal was irradiated with columnar defects to a matching field of $B_\Phi=2$ T which is twice as large as the matching field of the splayed defect samples, the pinning energy in the vortex liquid state at $T=91$ K is comparable to that of Y264 and Y265. This implies that the origin of the vortex liquid pinning mechanism for straight columnar defects may be similar to that of splayed defects.

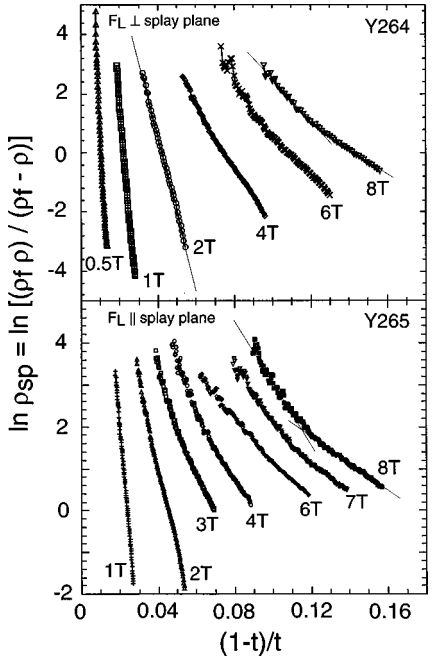

FIG. 6. Plot of $\ln(\rho_{\rm sp})$ vs $(1-t)/t$ showing regimes of activated behavior after irradiation for Y264 and Y265 at several magnetic fields parallel to the c axis.

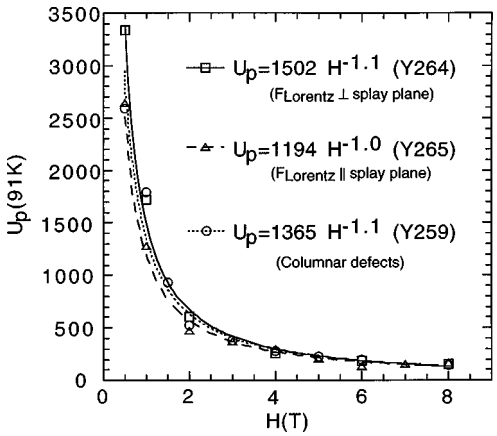

FIG. 7. Comparison of the field dependence of the vortex liquid pinning energy at $T=91.0$ K for vortex motion perpendicular (Y264) and parallel (Y265) to the splay plane. Also shown is the vortex liquid pinning energy for the straight columnar defect sample (Y259).

Finally, Fig. 8 shows a comparison of the heavy ion irradiated crystal with the electron irradiated crystal of Ref. 6. Both are normalized to $T=83$ K.

ANISOTROPIC PINNING OF THE VORTEX STATE

We investigated anisotropic pinning in the vortex liquid and solid state using angular dependent magnetoresistance measurements of the crystals before and after irradiation. In the unirradiated vortex solid state, we determined the pinning accommodation angle of the remnant strain field after detwinning. In the irradiated vortex liquid state, we determined the onset of anisotropic pinning and the pinning accommodation angle of the splayed and columnar defects. We found that the resistive pinning onset, described by the value of $\rho/\rho(T_{c0})$ at the onset of pinning, increases sharply below the dose matching field.

We argued earlier that the ''peak effect'' indicated by a minimum in the resistivity in the tail of the superconducting resistive transition for crystal Y264 for $H\|c$ before irradiation [Fig. 3(a)], was enhanced by pinning arising from remnant twin boundary strain fields. In order to check for any vestige of correlated pinning sites before irradiation which

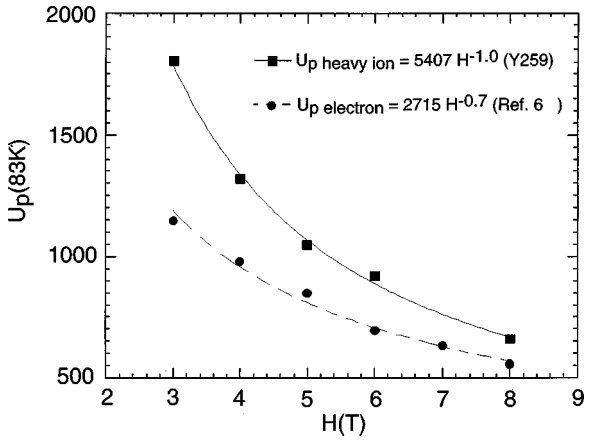

FIG. 8. Comparison of the field dependence of the vortex liquid pinning energy for columnar and point defects.

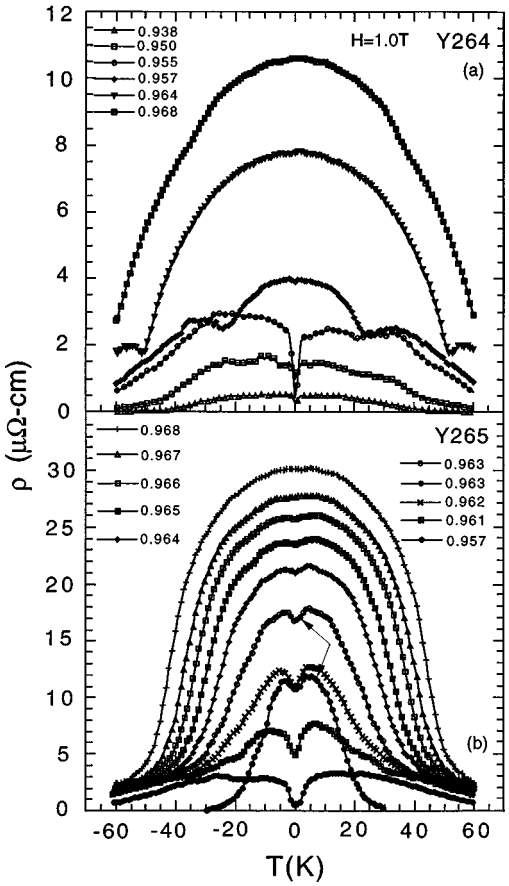

FIG. 9. (a) Angular dependence of the resistivity at various temperatures in a magnetic field of 1.0 T for crystals Y264 and Y265 before irradiation. The arrows in (b) indicate the resistivity at $t=0.963$ with measuring currents 0.83 A/cm^2 (closed circles) and 8.3 A/cm^2 (open circles).

may lead to anisotropic pinning, we measured the resistivity as a function of angle of the magnetic field from the c axis. The rotation plane was chosen to be perpendicular with the current direction in order to preserve a constant magnitude of the Lorentz force. Figure 9 shows the angular dependence of the resistivity for $H=1$ T at several temperatures above and below the vortex lattice melting temperature for crystal Y264 before irradiation. A sharp minimum at $\theta=0°$ is observed in the vortex solid state below T_m at $t=T/T_{c0}=0.954$. The anisotropic pinning accommodation angle of about 5° is consistent with the results of Fig. 3(b), where a tilt of the magnetic field of 5° from the c axis suppresses a large portion of the peak effect (i.e., minimum in the resistivity).

Figure 9(b) shows similar results for crystal Y265. The curves were obtained with a measuring current of 8.3 A/cm^2. Again, although no twin planes were detected with polarized light microscopy, we observe a shallow minimum in the resistivity at $\theta=0°$ ($H\|c$). The first appearance of the minima occurs close to $t=0.966$ and becomes more pronounced with decreasing temperature. The twin boundary pinning accommodation angle is also about 5°, comparable to that of very dilutely twinned crystals[34] and much less than that of densely twinned crystals where the accommodation angle at this field can be as large as 25°.[21] Furthermore, the onset of twin boundary pinning in this crystal is found only in the non-

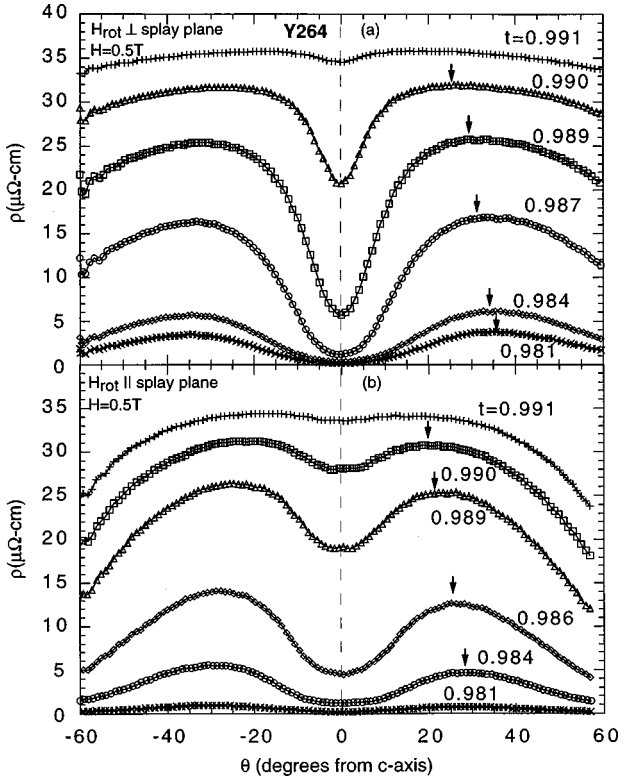

FIG. 10. Angular dependence of the resistivity for Y264 after irradiation at $H=0.5$ T and at several reduced temperatures $t=T/T_{co}$ for (a) tilt angles perpendicular to the splay plane, maintaining a constant Lorentz force magnitude on the vortices and for (b) tilt angles parallel to the splay plane. The arrows depict the pinning accommodation angle θ_{aco}.

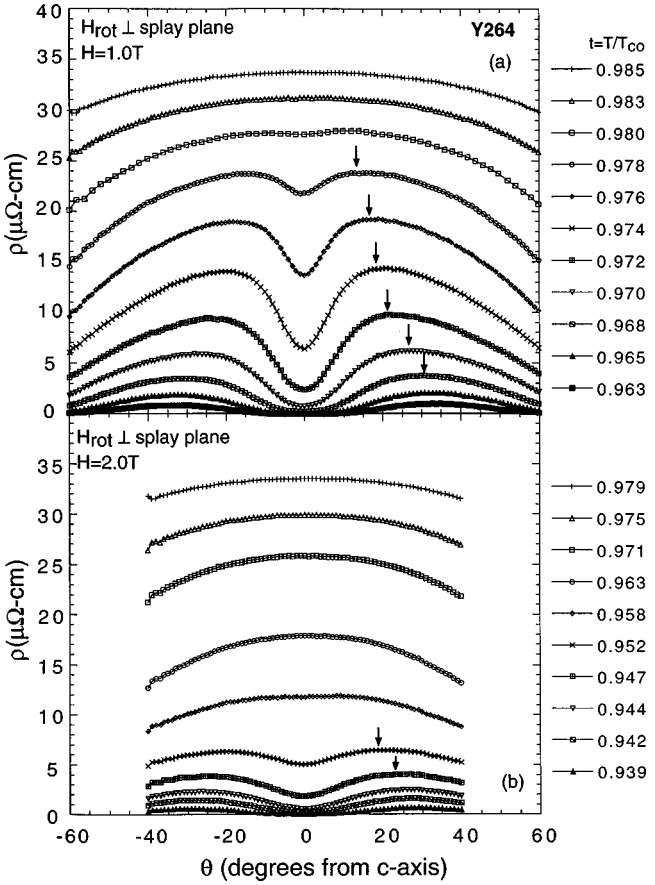

FIG. 11. Angular dependence of the resistivity for (a) $H=B_\Phi$ and (b) $H=2B_\Phi$ for tilt angles perpendicular to the splay plane (max. Lorentz force) for Y264.

Ohmic vortex solid state below T_m. This is clearly seen in Fig. 9(b) in the current dependence of the pinning accommodation angle for $H=1$ T at $T=90.11$ K measured with $J=0.83$ A/cm^2 (closed circles) and 8.3 A/cm^2 (open circles). The curve for $J=0.83$ A/cm^2 shows a smaller dissipation due to the reduced Lorentz force. On the other hand, the accommodation angle at this temperature of about 5° seems to be independent of the driving current. In contrast, in densely and dilutely twinned crystals where the twin boundaries were visible under a polarized microscope, the onset of twin boundary pinning is usually marked by a broad shoulder in $\rho(T)$ for $H\|c$ at higher temperatures in the ohmic vortex liquid state and a pronounced dip in $\rho(\theta)$ below the shoulder. No twin boundary pinning in the *liquid* state was observed in Y264, Y265, or Y259. We surmise that the anisotropic pinning is due to weak remnant strain fields along the twin boundary direction remaining after the detwinning process.[25] The fact that twin boundary pinning is absent in the vortex liquid state and only observed in the vortex solid state when a finite shear modulus is present suggests the very weak nature of remnant twin boundary pinning in these untwinned crystals.

A large anisotropic pinning in the vortex liquid state was observed after irradiation. The onset of anisotropic vortex liquid pinning by the splayed defects after irradiation is confirmed by the angular dependent pinning shown in Fig. 10 for Y264 for $H=0.5$ T. Figure 10(a) shows $H_{rot}\perp$ splay plane. In this geometry, the applied magnetic field is rotated in a plane perpendicular to the splay plane, maintaining a maximum Lorentz force at all angles. Data are taken for several reduced temperatures. At $t=0.991$, a slight indication of pinning is observed as a minimum develops at $\theta=0°$ $(H\|c)$. A pinning accommodation angle θ_{acc} for splayed defects can be identified as half the angle between the two maxima on either side of $\theta=0°$. With decreasing temperature, the width of the minimum increases up to $\theta_{acc}=\pm 35°$.

Figure 10(b) shows $H_{rot}\|$splay plane. In this geometry, the Lorentz force continuously decreases as the applied magnetic field is tilted within the plane of the splayed defects from the c axis towards the direction of the measuring current along the b axis. Due to the reduced Lorentz force, a reduction in the dissipation is observed compared to the maximum Lorentz force geometry. The minimum also appears to be shallower. We also observe a small reduction in the pinning accommodation angle from $\theta_{acc}=35°$ to 30° as indicated by the arrows in the figure. From this type of measurement, we can deduce the onset temperature of anisotropic vortex pinning in the liquid state. For $H=0.5$ T, the onset lies slightly above $t=0.991$, very close to T_{c0} and at $\rho/\rho_n\sim 0.92$. For both rotations, we observe only one minima at $\theta=0°$ $(H\|c)$, although the columnar tracks are splayed at $\pm 10°$ from the c axis.

Figure 11 shows the angular dependence of the resistivity for $H=B_\Phi$ and $2B_\Phi$ for Y264. Compared to $H=B_\Phi/2$ of

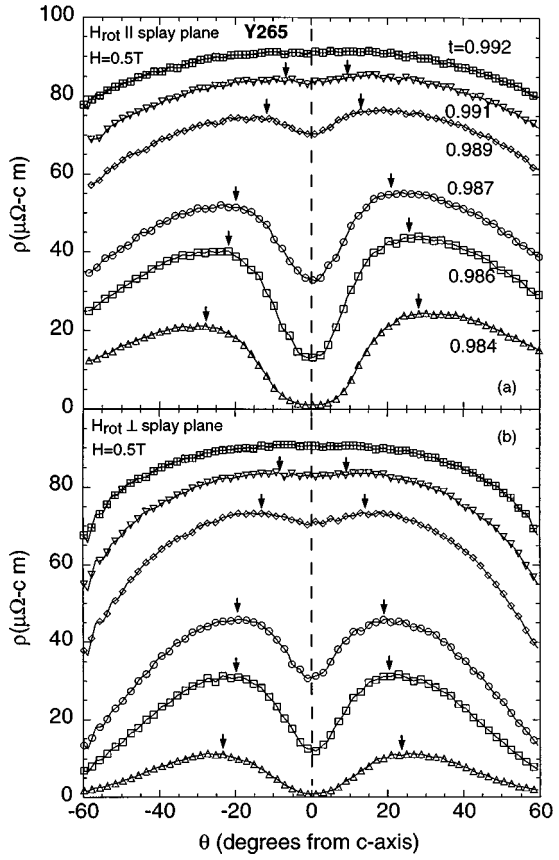

FIG. 12. Angular dependence of the resistivity at $H=0.5$ T for Y265 after irradiation. The top panel (a) is for tilt angles perpendicular to the splay plane, maintaining a constant Lorentz force on the vortices. The bottom panel (b) is for tilt angles parallel to the splay plane.

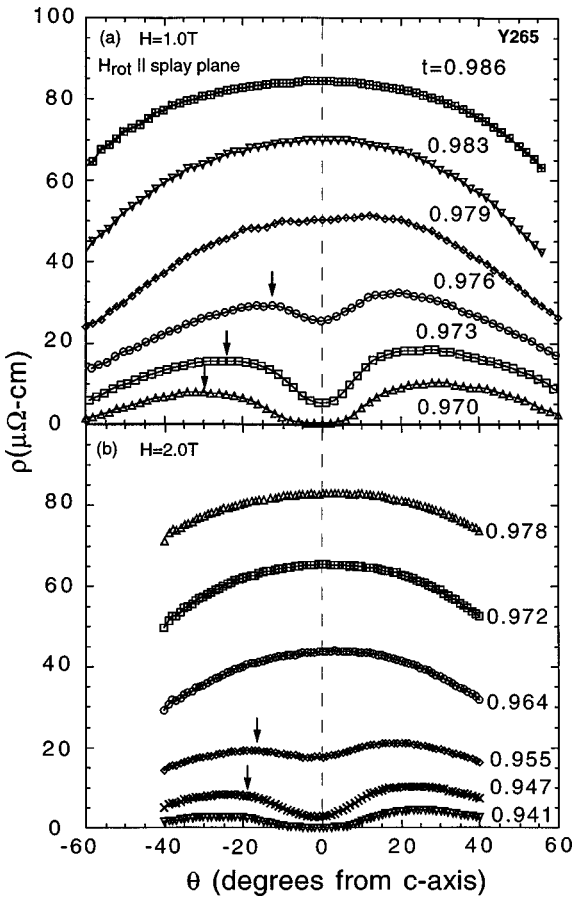

FIG. 13. Angular dependence of the resistivity for (a) $H=B_\Phi$ and (b) $H=2B_\Phi$ for tilt angles perpendicular to the splay plane (max. Lorentz force) for Y265 after irradiation.

Fig. 10(a) the minimum becomes shallower with increasing magnetic field. Furthermore, the pinning accommodation angle, $\theta_{\rm acc}$, also decreases with increasing field (i.e., max. $\theta_{\rm acc}\sim 25°$ for $H=2B_\Phi$). This can be explained by the change in vortex density with respect to the total defect density with increasing magnetic field. Above the matching field, the vortices outnumber the irradiation induced pin sites and hence the effect of anisotropic pinning due to the splayed defects decreases. This is consistent with the decrease in the onset temperature of anisotropic pinning and the decrease in the depth of the minima at $\theta=0°$ in the vortex liquid state with increasing magnetic field. For example, for $H=1$ T, the minimum at $\theta=0°$ develops near $t=0.980$, where $\rho/\rho_n\sim 0.75$, and reduces to $t=0.952$ where $\rho/\rho_n\sim 0.22$ for $H=2$ T. At $H=4$ T, the onset of pinning drops to $t=0.913$ where $\rho/\rho_n\sim 0.14$.

Figure 12(a) shows comparable data for Y265 ($F_L\|$splay plane) at $H=0.5$ T. Here, $H_{\rm rot}\|$splay plane corresponds to the maximum Lorentz force configuration. The onset of splayed columnar defect pinning is clearly observed by the onset of the minimum at $\theta=0°$ ($H\|c$) between $0.992<t<0.991$. This temperature corresponds to the temperature $T_{\rm sp}$ of the onset of splayed defect pinning observed in Fig. 4. The lower panel shows that the accommodation angles for field rotations perpendicular to the splay plane are slightly smaller than the accommodation angles for field rotations parallel to the splay plane for the same temperature values, consistent with the difference in Lorentz force for the two orientations. For example, at $t=0.984$, $\theta_{\rm acc}\sim 28°$ for $H_{\rm rot}\|$splay plane compared with $\theta_{\rm acc}\sim 24°$ for $H_{\rm rot}\perp$splay plane. Figure 13 shows similar data for $H=B_\Phi$ and $2B_\Phi$. Similar to Y264, the pinning accommodation angle $\theta_{\rm acc}$ decreases with increasing field and the minimum at $\theta=0°$ becomes shallower. These accommodation angles after irradiation for Y264 and Y265 are much larger than the remnant twin boundary pinning angle of $\theta_{\rm TB}=5°$ observed before irradiation and the onset temperatures for $\theta_{\rm acc}$ are in the ohmic vortex liquid regime, whereas the remnant twin boundary pinning before irradiation occurred only below the melting temperature in the vortex solid regime.

Figure 14 shows the angular dependence of the resistivity for Y259 (columnar defect sample) after irradiation to a matching field of $B_\Phi=2$ T. Here, the angle of rotation is always perpendicular to the measuring current, resulting in the maximum Lorentz force configuration for all angles. The pinning accommodation angle for straight columnar defects for $H=1$ T is shown in Fig. 14(b). The pinning accommodation angle is about $\theta_{\rm acc}\sim 35°$ at $T=91.61$ K. This value is much smaller than the pinning accommodation angle of $\sim 70°$, obtained in another untwinned $YBa_2Cu_3O_{7-\delta}$ crystal irradiated with uranium ions to the same matching field[27]

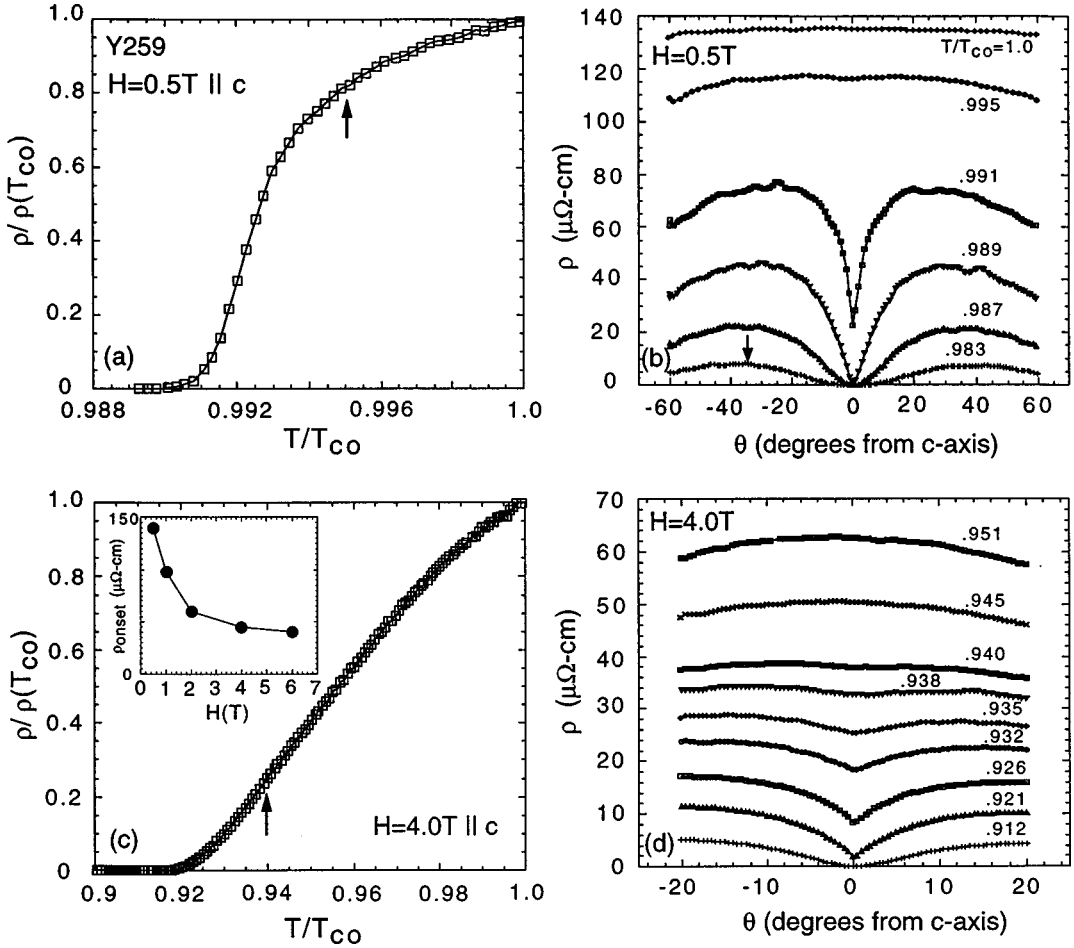

FIG. 14. (a) Temperature dependence of the resistivity after irradiation for Y259 at $H=0.5\ \mathrm{T}\|c$. The arrow depicts the onset of anisotropic pinning due to columnar defects obtained from (b) the angular dependence of the resistivity at $H=0.5$ T. (c) Temperature dependence of the resistivity at $H=4\ \mathrm{T}\|c$. The arrow depicts the onset of anisotropic pinning due to columnar defects obtained from (d) the angular dependence of the resistivity at $H=4$ T. Inset: magnetic field dependence of the resistive onset of anisotropic pinning.

suggesting that ion size may be used to control the pinning strength of columnar defects. The onset of anisotropic pinning occurs near $T=92.74$ K for $H=1$ T, where a very weak depression in the resistivity is observed at $\theta=0°$. This temperature corresponds to a $\rho/\rho(T_{c0})$ value of nearly 80% as shown in Fig. 14(a). At higher magnetic fields, the pinning accommodation angle decreases and the onset of anisotropic pinning reduces to $\rho/\rho(T_{c0})\sim 20\%$ for $H=4$ T [see Figs. 14(c) and 14(d)]. The inset to Fig. 14(c) shows magnetic field dependence of the resistive onset point for anisotropic pinning due to columnar defects. We observe a sharp rise of the pinning onset point below the matching field. Our results indicate that pinning becomes dramatically less effective for magnetic fields greater than the matching field where vortices outnumber the columnar defects.

ANISOTROPIC CRITICAL CURRENTS

We investigated the critical current of the vortex solid state before and after irradiation from E-J curves obtained from dc transport measurements. We observed a crossing in the measured pre- and postirradiation temperature dependent critical current values, consistent with the irreversibility line behavior reported above. We find the barriers for vortex motion to be larger for motion perpendicular to the splay planes than for motion parallel to the splay planes. No crossing of the pre- and postirradiation temperature dependent critical current values were observed for the crystal irradiated with parallel columnar defects.

The voltage-current curves of crystal Y265 at several temperatures before irradiation for $H=1.0\ \mathrm{T}\|c$ are shown in Fig. 15. The transition from vortex-liquid Ohmic behavior to a vortex solid non-Ohmic behavior at lower temperatures oc-

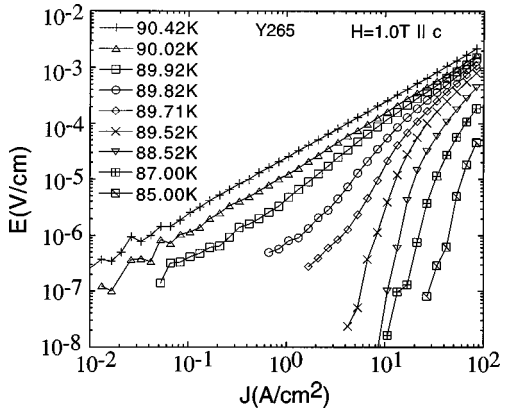

FIG. 15. E vs J curves at various temperatures for Y265 at $H=1\ \mathrm{T}\|c$ before irradiation.

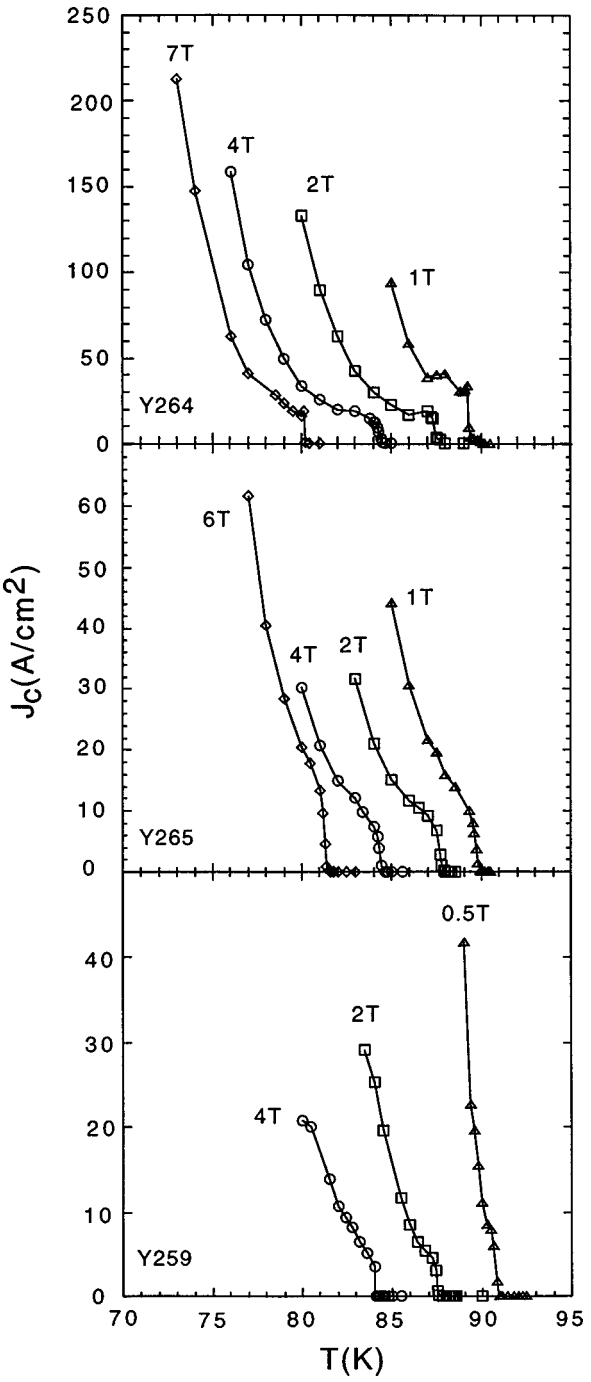

FIG. 16. Temperature dependence of the critical current before irradiation for Y264, Y265, and Y259 at various magnetic fields applied parallel to the *c* axis.

curs through an ''*S*'' shaped transition region. At $T=90.42$ K, the log E vs log J curve display Ohmic behavior as shown by a power law curve fit I^{α} with $\alpha=1$. Below this temperature, the curves deviate from linearity and evolve into an *S*-shape associated with the vortex lattice melting transition.[40] At lower temperatures, the E-J curves depict a strong downward curvature. Using a $E=1\ \mu$V/cm criterion, we determined the critical current as a function of temperature for several magnetic fields as shown in Fig. 16 for Y264, Y265, and Y259 before irradiation. For each $J_c(T)$ curve, there is a sharp increase in the critical current at the freezing temperature followed by a smooth exponential increase in the critical current with decreasing temperature. The behavior of the critical current just below the melting temperature for Y264 and Y265 follows a power-law behavior with $J_c=J_0T^s$ where $s\sim 28\pm 3$ for all fields measured, in good agreement with magnetic measurements by Senoussi *et al.*,[41] where they observed an exponential behavior at low temperatures and a power law behavior near T_c.

The temperature dependence of the critical current for crystal Y264 shows a peak effect for $H=1$, 2, and 7 T, which corresponds in temperature to the resistive minimum observed in Fig. 3. The critical current values of crystal Y264 are, on average, about 60% larger than those of crystal Y265. This indicates that although Y264 demonstrated a smaller normal state resistivity than Y265, the remnant twin boundary pinning in Y264 is stronger than in Y265. This is consistent with the observation of a peak effect in Y264.

The critical currents for both crystals increased dramatically after irradiation which induced splayed defects in both Y264 and Y265. Figure 17 shows the temperature dependence of the critical current compared to that of the preirradiation behavior at magnetic fields above and below the matching field of $B_{\Phi}=1$ T for Y265. For all fields, the critical current rises sharply at the irreversibility temperature and continues to increase rapidly unlike the slow rise in J_c observed below T_m in the preirradiation behavior in Fig. 16. This indicates that the critical current is significantly enhanced after irradiation with splayed columnar defects. However, close observation shows that although at low fields, the irradiated sample shows a critical current much higher in magnitude than the preirradiated case for a fixed temperature and field, at high fields there is a crossover and the onset of the critical current occurs at a temperature well below the melting temperature of the preirradiated case. This is consistent with the zero resistance temperature of the irradiated crystal compared to its pre-irradiated value as shown in Fig. 4(b) and the crossing of the irreversibility lines near $2B_{\Phi}$ shown in Fig. 5(b).

The temperature dependence of the critical current for Y264 and Y259 before and after irradiation is shown in Fig. 18. For crystal Y264, comparison of the critical current before and after irradiation at $H=1$ T and 4 T shows that its behavior is similar to that of crystal Y265 described above. On the other hand, the critical current and its onset temperature after irradiation for crystal Y259 are always higher than their values before irradiation for all fields measured as shown in Fig. 18(b).

DISCUSSION AND ANALYSIS

We have measured the vortex pinning characteristics of two untwinned $YBa_2Cu_3O_{7-\delta}$ single crystals before and after they were subjected to heavy ion irradiation in a splayed geometry and one untwinned crystal subjected to irradiation inducing parallel columnar defects. One of the salient features which we observe is the crossing of the irreversibility lines before and after irradiation. The crossing suggests that splayed columnar defects are effective in pinning the vortex liquid only at high temperatures and below about twice the

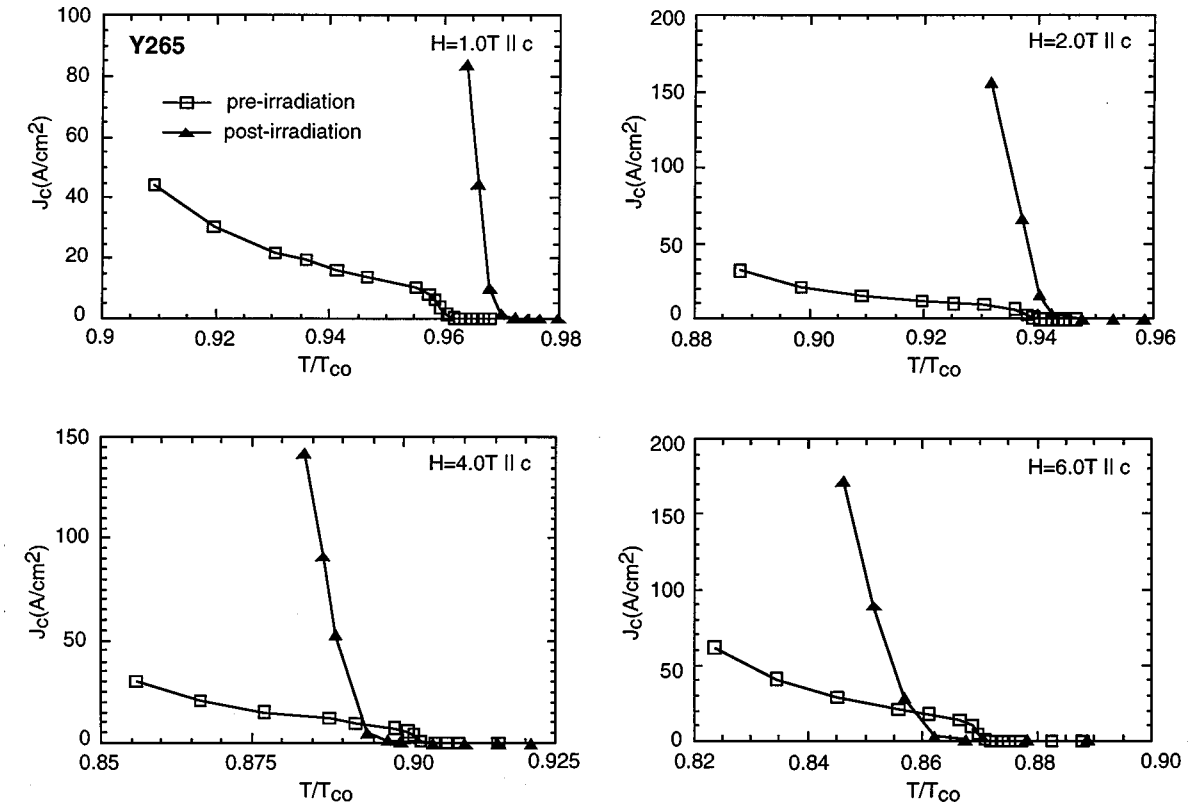

FIG. 17. Temperature dependence of the critical current before (open squares) and after (closed triangles) irradiation for crystal Y265 at $H=1$, 2, 4, and 6 T$\|c$.

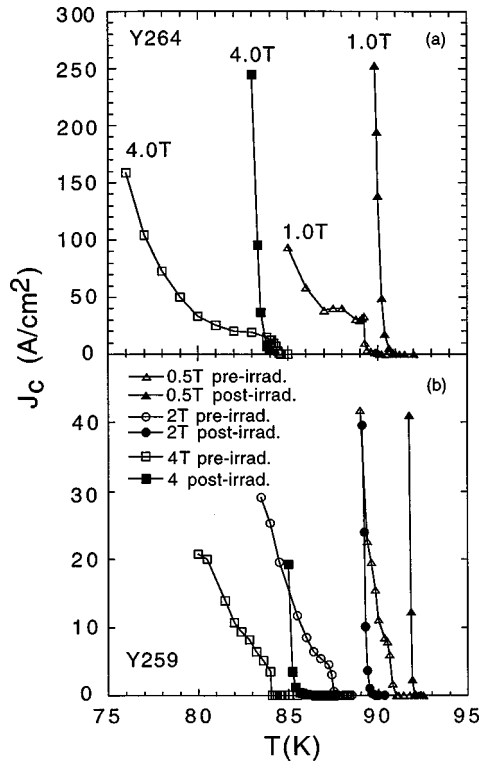

FIG. 18. Temperature dependence of the critical current before (open symbols) and after (closed symbols) irradiation for (a) crystal Y264 with splayed defects and (b) crystal Y259 with columnar defects for various magnetic fields parallel to the c axis.

matching field. At higher fields when the density of vortices exceeds the density of columnar defects, splayed defects seem to lose their ability to pin the liquid effectively. However, the critical currents observed in the vortex solid state just below the irreversibility line after irradiation show large enhancements over the preirradiation values. This can be explained if the splayed defects induce large topological entanglement[42] in the vortex liquid state. In the entangled state after irradiation, the vortices are unable to disentangle and to form an Abrikosov lattice at the freezing temperature, and thus we no longer observe the sharp ''kink'' in the resistivity associated with the first order vortex freezing transition (see Fig. 4). At lower temperatures, below the preirradiation–first order melting temperature, the vortices eventually freeze into an entangled solid. The topologically entangled solid has a larger shear viscosity than the shear modulus of a vortex lattice and hence the critical current is enhanced.

The crossing of the pre- and postirradiation irreversibility lines seems to be associated with the splayed geometry which promotes vortex entanglement. This crossing is not observed in crystal Y259 with straight columnar defects induced by irradiation with 3.9 GeV $^{197}Au^{29+}$ to a matching field of $B_\Phi=2$ T$\|c$. However, the close $1/H$ behavior observed in the straight columnar defect sample suggests that vortex entanglement may also play a role in the pinning of the vortex liquid state as shown below.

The $1/H$ behavior found in the field dependence above the matching field of the vortex liquid state pinning energy for all the irradiated crystals can be explained by assuming an

entangled vortex state. We use the concept of a pinned ''vortex lace,'' [22] a densely entangled vortex configuration which is firmly fastened by a moderate number of strong parallel or splayed columnar defects. Because of the dense entanglement, the pinning energy of the trapped vortices is distributed nearly evenly among all the vortices enclosed by an ''elementary cell'' of the defect structure. This elementary cell includes vortices within an area, d^2, where d is the defect spacing. Therefore, the average cost to remove a representative vortex from the splayed defect potential well can be estimated as

$$E_p = U_0 l (a_0^2/d^2) \ln(d/r_0), \tag{1}$$

where U_0 is the pinning energy of the splayed defect per unit length, r_0 is the radius of the columnar defect, $a_0 = (\Phi_0/B)^{1/2}$ is the vortex spacing with Φ_0, the flux quantum, and l is the length of the liberated vortex segment. To free this segment, the vortex must bend, and the corresponding vortex bending energy

$$E_b = \varepsilon_1 a_0^2 / l, \tag{2}$$

where $\varepsilon_1 = \varepsilon(\Phi_0/4\pi\lambda)^2 \ln(\lambda/\xi)$ is the vortex line tension energy, $a_0 = (\Phi_0/B)^{1/2}$ is the vortex spacing, λ and ξ are the superconducting penetration and coherence length respectively, and ε is the anisotropy parameter. The total energy cost for depinning the vortex lace is therefore $E = E_p + E_b$, optimized with respect to the length of the fluctuating segment l. This yields

$$l_{\text{opt}} = d[\varepsilon_1 / U_0 \ln(d/r_0)]^{1/2} \tag{3}$$

and substituting into E gives

$$E = 2(a_0^2/d)[U_0 \varepsilon_1 \ln(d/r_0)]^{1/2}. \tag{4}$$

Using the relation $\varepsilon_1 = \varepsilon^2 \varepsilon_0$ and the estimate $U_0 \sim \varepsilon_0$, we obtain

$$E = 2\varepsilon\varepsilon_0 (a_0^2/d)[\ln(d/r_0)]^{1/2}, \tag{5}$$

where $\varepsilon \sim 1/7$ for $YBa_2Cu_3O_{7-\delta}$ and $\varepsilon_0 = (\Phi_0/4\pi\lambda)^2$. Using characteristic values $B = B_\Phi = 1$ T, $a_0 = 450$ Å, $d \sim 450$ Å, $r_0 \sim 30$ Å,[43] and $\lambda_0 = 1400$ Å, we obtain $E(T = 0\text{ K}) = E_0 \sim 21333$ K from Eq. (5) above. For $T = 91$ K, $E_p = E_0(1 - T/T_{c0}) = 546$ K. This is in fair agreement with our measured value of $U_p(91\text{ K}) = 1280$ K shown in Fig. 7 and correctly predicts the observed $1/H$ dependence.

Note that this simple vortex lace model does not take into account the geometry of the columnar defects and thus should also be applicable to the case of straight columnar defects for $H > B_\Phi$, and indeed, crystal Y259 also exhibits $1/H$ behavior as was demonstrated in Figs. 7 and 8. Perhaps parallel columnar defects could also promote topological vortex entanglement when vortices are driven by a Lorentz force which induces a relative change in velocity $\delta v/v$ between the pinned and interstitial vortices. Of course, we cannot conclusively prove the existence of vortex entanglement. However, our experimental results are consistent with a topological vortex entanglement picture.

We can also analyze the anisotropic pinning energy in the vortex liquid state of the irradiated crystals from their pinning accommodation angles, θ_{acc}. Figure 19 shows the temperature dependence of the depinning angles for both crystals Y264 and Y265. We estimate the strength of the pinning energy per unit length U_p' from θ_{acc}, following the trapped vortex geometry introduced by Sonin[44] for the case of twin boundary pinning and which we recently extended to the case of columnar defect pinning.[27] At high temperatures, the pinning accommodation angle determined by thermal fluctuations and U_p' can be estimated from equation

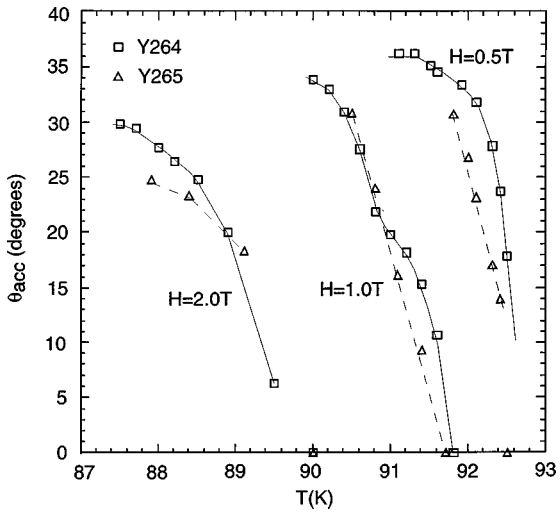

FIG. 19. Temperature dependence of the pinning accommodation angle for crystal Y264 and Y265. The lines are a guide to the eye.

$$Up' \sim \varepsilon_0 \left[\frac{2 k_B T \tan \theta_{\text{acc}}}{\varepsilon_0 a_0} \right]^{2/3}. \tag{6}$$

Using this analysis, we determined the pinning energy per unit length at $t = T/T_{c0} = 0.975$ for Y264 for $H = 0.5$ T ($\theta_{\text{acc}} = 36°$) and 1 T ($\theta_{\text{acc}} = 19.1°$). We find $U_p' = 5.97 \times 10^7$ K/cm and 4.59×10^7 K/cm, respectively. These values lie between the pinning energies obtained for uranium ion induced parallel columnar defects and densely twinned crystals.[27] From the values of U_p and U_p', we can determine the pinned vortex length. For $T = 91.1$ K, $U_p(H = 0.5\text{ T}) \sim 3400$ K and $U_p' = 5.97 \times 10^7$ K/cm, therefore the trapped length $l_p \sim U_p/U_p' \sim 5700$ Å, comparable to several hundred unit cells.

Figure 20 shows a direct comparison of the temperature dependence of the critical current for Y264 and Y265. It clearly shows that the critical current is larger and increases at a more rapid rate for Lorentz force induced motion perpendicular to the splay plane (Y264) than for motion parallel to the splay plane (Y265). The slope of J_c vs T for Y264 is approximately 3 times larger than the slope for Y265. This suggests that a plane of intersecting columnar defects poses a large pinning barrier for motion perpendicular to the plane. Motion parallel to the splay plane can occur through transfer of a vortex from one columnar defect to another at their intersection point. This result is compatible with the observation of anisotropic twin boundary pinning in densely twinned $YBa_2Cu_3O_{7-\delta}$ crystals.[21] It is also consistent with the lower vortex liquid pinning energy ob-

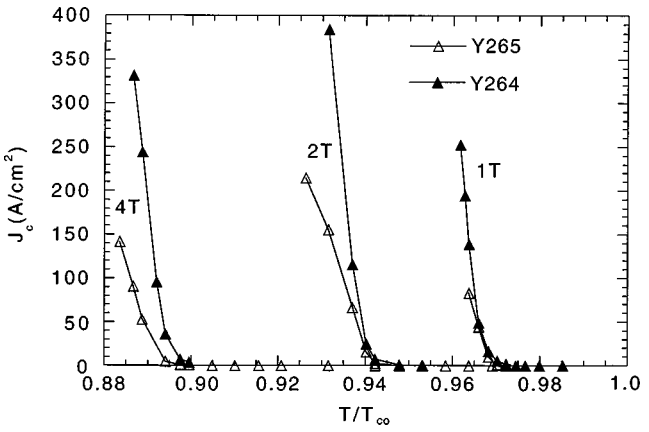

FIG. 20. Comparison of the temperature dependence of the critical current after irradiation for crystal Y264 ($F_{\mathrm{Lorentz}}\perp$ splay plane) and Y265 ($F_{\mathrm{Lorentz}}\|$splay plane) for $H=1$, 2, and 4 T$\|c$.

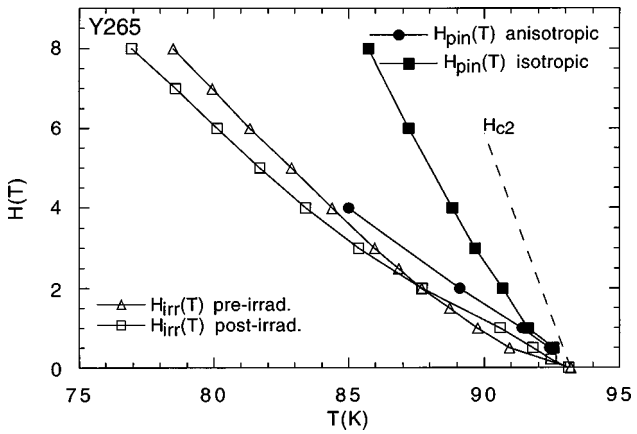

FIG. 21. Phase diagram for the splayed columnar defected crystal Y265 at $H\|c$, showing the irreversibility lines before and after irradiation and the onset of anisotropic and isotropic pinning. A typical upper critical field H_{c2} line for $YBa_2Cu_3O_{7-\delta}$ is also shown for comparison.

served for motion parallel to the splay plane (Y265) compared to motion perpendicular to the splay plane (Y264) shown in Fig. 7.

Finally, the onset of pinning due to splayed defects in the vortex liquid state was initially obtained from the divergence of the two normalized resistivity curves taken before and after irradiation at a constant magnetic field for $H\|c$ (see Fig. 4). The onset temperature of *anisotropic* pinning in the liquid state was obtained directly from the angular dependence of the resistivity which showed the onset of a minimum at $\theta=0°$ ($H\|c$) (see Figs. 10–14). For magnetic fields below the matching field, the onset of pinning obtained from the two methods above coincide very well. However, for fields above the matching field, the onset of anisotropic pinning lies below that of isotropic pinning, underlining the behavior of excess vortices over the number of columnar defects. The fact that the deviation occurs just above the matching field is consistent with our observation that the maximum shift in the irreversibility line after irradiation also occurs at this field value. The complete phase diagram with the onset of *isotropic* and *anisotropic* pinning is shown in Fig. 21 for crystal Y265.

SUMMARY

In conclusion, we have investigated the vortex pinning behavior in splayed and straight columnar defects in clean untwinned crystals of $YBa_2Cu_3O_{7-\delta}$ where the competing effects of twin boundary pinning are absent. We observe several features which are linked to the matching field. We observe (i) a crossing of the irreversibility lines of the pre- and postirradiated samples at twice the matching field, (ii) the largest temperature shift in the postirradiated sample near the matching field, (iii) a jump in the resistive pinning value ρ/ρ_n just below the matching field, and (iv) the onset of isotropic and anisotropic pinning to coincide below the matching field. Using an interpolation formula, we determined the field dependence of the vortex liquid pinning energy and introduced a ''vortex lace'' pinning model which accounts for the observed $1/H$ dependence. Comparison with a parallel columnar defected untwinned crystal shows that the $1/H$ dependence is also present in this case, however, the crossing of the irreversibility lines is not observed. Furthermore, the vortex liquid pinning energy for the straight columnar defect sample is similar to that of the splayed defect samples, even though the matching field is twice as large. This suggests that vortex liquid pinning in the splayed and columnar defect samples may have a similar origin. In addition, the fact that the splayed defect sample (Y264) with $F_L\perp$ splay plane and with a lower matching field has a slightly higher vortex liquid pinning energy than the straight columnar defect sample also indicates that splayed defects are more effective in promoting entanglement. Despite the depression of the irreversibility lines above $2B_\Phi$ for the splayed defect crystals, values of the critical current and its temperature dependence are dramatically enhanced in the vortex solid state. We speculate that topological entanglement induced by the splayed defects is responsible for the increased critical current. The splayed defects pin the vortices more strongly against motion perpendicular to the splay plane than for parallel motion. At fields above B_Φ, isotropic pinning of the vortex liquid begins to manifest itself at temperatures above the onset of anisotropic pinning due to splayed defects. Finally, we estimated the trapped vortex pinning length due to splayed defects from the vortex liquid pinning energy and the pinning accommodation angle.

ACKNOWLEDGMENTS

We thank Dr. Raman Anantaraman for providing the irradiation facility at the National Superconducting Cyclotron Laboratory. This work was supported by the U.S. Department of Energy, BES—Materials Science under Contract No. W-31-109-ENG-38 (W.K.K., V.M.V., G.W.C.), the NSF-Science and Technology Center for Superconductivity under Contract No. DMR91-20000 (L.M.P., A.M.P.), the National Science Foundation under Contract No. PHY-9528844 (R.M.R.) and DMR-9624047 (L.M.P.), and the Faculty Research Participation Program administered by the Argonne Division of Educational Programs (L.M.P.).

[1] L. Civale, A. D. Marwick, T. K. Worthington, M. A. Kirk, J. R. Thompson, L. Krusin-Elbaum, Y. Sun, J. R. Clem, and F. Holtzberg, Phys. Rev. Lett. **67**, 648 (1991).
[2] M. Konczykowski, F. Rullier-Albenque, E. R. Yacoby, A. Shaulov, Y. Yeshurun, and P. Lejay, Phys. Rev. B **44**, 7167 (1991).
[3] L. M. Paulius, C. C. Almasan, and M. B. Maple, Phys. Rev. B **47**, 11627 (1993).
[4] J. Giapintzakis, W. C. Lee, J. P. Rice, D. M. Ginsberg, I. M. Robertson, R. Wheeler, M. A. Kirk, and M.-O. Ruault, Phys. Rev. B **45**, 10677 (1992).
[5] J. Giapintzakis, M. A. Kirk, W. C. Lee, J. P. Rice, D. M. Ginsberg, I. M. Robertson, and R. L. Wheeler, in *Layered Superconductors: Fabrication, Properties and Applications*, edited by D. T. Shaw *et al.*, MRS Symposia Proceedings No. 275 (Materials Research Society, Pittsburgh, 1992), p. 741.
[6] J. A. Fendrich, W. K. Kwok, J. Giapintzakis, C. J. van der Beek, V. M. Vinokur, S. Fleshler, U. Welp, H. K. Viswanathan, and G. W. Crabtree, Phys. Rev. Lett. **74**, 1210 (1995).
[7] L. Civale, A. D. Marwick, M. W. McElfresh, T. K. Worthington, A. P. Malozermoff, F. H. Holtzberg, J. R. Thompson, and M. A. Kirk, Phys. Rev. Lett. **65**, 1164 (1990).
[8] L. M. Paulius, R. E. Shamu, S. Ferguson, M. C. de Andrade, and M. B. Maple, Appl. Phys. Lett. **71**, 3415 (1997).
[9] B. M. Vlcek, M. C. Frischherz, H. K. Viswanathan, U. Welp, G. W. Crabtree, and M. A. Kirk, IEEE Trans. Appl. Supercond. **3**, 1491 (1993).
[10] D. S. Fisher, M. P. A. Fisher, and D. A. Huse, Phys. Rev. B **43**, 130 (1991).
[11] M. P. A. Fisher, Phys. Rev. Lett. **62**, 1415 (1989).
[12] D. R. Nelson and V. M. Vinokur, Phys. Rev. Lett. **68**, 2398 (1992).
[13] D. R. Nelson and V. M. Vinokur, Phys. Rev. B **48**, 13060 (1993).
[14] T. Hwa *et al.*, Phys. Rev. Lett. **71**, 3545 (1993).
[15] L. Civale, L. Krusin-Elbaum, J. R. Thompson, R. Wheeler, M. A. Kirk, and C. Field, Physica C **235–240**, 2969 (1994).
[16] K. Krusin-Elbaum, J. R. Thompson, R. Wheeler, A. D. Marwick, C. Li, S. Patel, D. T. Shaw, P. Lisowski, and J. Ullmann, Appl. Phys. Lett. **64**, 3331 (1994).
[17] H. Safar, J. H. Cho, S. Fleshler, M. P. Maley, J. O. Willis, J. Y. Coulter, J. L. Ullmann, G. N. Riley, Jr., M. W. Rupich, J. R. Thompson, and L. Krusin-Elbaum, Appl. Phys. Lett. **67**, 130 (1995).
[18] J. O. Willis, H. Safar, J. H. Choi, J. Y. Coulter, M. P. Maley, P. A. Smith, D. S. Phillips, J. L. Ullmann, G. N. Riley, Jr., M. W. Rupich, and S. Fleshler, in *Advances in Superconductivity VIII*, edited by H. Hayakawa and Y. Enomoto (Springer-Verlag, Tokyo, 1996), Vol. 1, p. 509.
[19] D. S. Reed, N.-C. Yeh, W. Jiang, U. Kriplani, M. Konczykowski, and F. Holtzberg, Int. J. Mod. Phys. B **10**, 2723 (1996).
[20] L. Krusin-Elbaum, A. D. Marwick, R. Wheeler, C. Feild, V. M. Vinokur, G. K. Leaf, and M. Palumbo, Phys. Rev. Lett. **76**, 2563 (1996).
[21] S. Fleshler, W. K. Kwok, U. Welp, V. M. Vinokur, M. K. Smith, J. Downey, and G. W. Crabtree, Phys. Rev. B **47**, 14448 (1993).
[22] W. K. Kwok, L. M. Paulius, V. M. Vinokur, A. M. Petrean, R. M. Ronningen, and G. W. Crabtree, Phys. Rev. Lett. **80**, 600 (1998).
[23] M. A. Moore and N. K. Wilkin, Phys. Rev. B **50**, 10294 (1994).
[24] D. L. Kaiser, F. Holtzberg, B. A. Scott, and T. R. McGuire, Appl. Phys. Lett. **51**, 1040 (1987).
[25] U. Welp, M. Grimsditch, H. You, W. K. Kwok, M. M. Fang, G. W. Crabtree, and J. Z. Liu, Physica C **161**, 1 (1989).
[26] J. P. Biersack and J. F. Ziegler, Transport of Ions in Matter (TRIM)-Monte Carlo Simulation Program, Ver. 91.14.
[27] L. M. Paulius, J. A. Fendrich, W. K. Kwok, A. E. Koshelev, V. M. Vinokur, and G. W. Crabtree, Phys. Rev. B **56**, 913 (1997).
[28] H. Safar, P. L. Gammel, D. A. Huse, D. J. Bishop, J. P. Rice, and D. M. Ginsberg, Phys. Rev. Lett. **69**, 824 (1992).
[29] W. K. Kwok, S. Fleshler, U. Welp, V. M. Vinokur, J. Downey, and G. W. Crabtree, Phys. Rev. Lett. **69**, 3370 (1992).
[30] M. Charalambous, J. Chaussy, and P. Lejay, Phys. Rev. B **45**, 5091 (1992).
[31] U. Welp, J. A. Fendrich, W. K. Kwok, G. W. Crabtree, and B. W. Veal, Phys. Rev. Lett. **76**, 4809 (1996).
[32] A. B. Pippard, Philos. Mag. **19**, 217 (1969).
[33] S. H. Autler, E. S. Rosenblum, and K. H. Gooen, Phys. Rev. Lett. **9**, 489 (1962).
[34] W. K. Kwok, J. A. Fendrich, C. J. van der Beek, and G. W. Crabtree, Phys. Rev. Lett. **73**, 2614 (1994).
[35] G. W. Crabtree, M. B. Maple, W. K. Kwok, J. Herrmann, J. A. Fendrich, N. R. Dilley, and S. H. Han, Phys. Essays **9**, 628 (1996).
[36] J. A. Fendrich, U. Welp, W. K. Kwok, A. E. Koshelev, G. W. Crabtree, and B. W. Veal, Phys. Rev. Lett. **77**, 2073 (1996).
[37] D. T. Fuchs, E. Zeldov, M. Rappaport, S. Tamegai, S. Ooi, and H. Shtrikman, Nature (London) **391**, 373 (1998).
[38] G. Blatter *et al.*, Rev. Mod. Phys. **66**, 1125 (1994).
[39] V. M. Vinokur, M. V. Feigel'man, V. B. Geshkenbein, and A. I. Larkin, Phys. Rev. Lett. **65**, 259 (1990).
[40] W. K. Kwok, J. Fendrich, S. Fleshler, U. Welp, J. Downey, and G. W. Crabtree, Phys. Rev. Lett. **72**, 1092 (1994).
[41] S. Senoussi, M. Oussena, G. Collin, and I. A. Campbell, Phys. Rev. B **37**, 9792 (1988).
[42] D. R. Nelson, Phys. Rev. Lett. **60**, 1973 (1988).
[43] A. D. Marwick, L. Civale, L. Krusin-Elbaum, R. Wheeler, J. R. Thompson, T. K. Worthington, M. A. Kirk, Y. R. Sun, H. R. Kerchner, and F. Holtzberg, Nucl. Instrum. Methods Phys. Res. B **81/81**, 1143 (1993); R. Wheeler (unpublished).
[44] E. B. Sonin, Phys. Rev. B **48**, 10487 (1993).